Surface & Coatings Technology 404 (2020) 126477

Contents lists available at ScienceDirect

Surface & Coatings Technology

journal homepage: www.elsevier.com/locate/surfcoat

Effect of microstructure and porosity of AlSi10Mg alloy produced by selective laser melting on the corrosion properties of plasma electrolytic oxidation coatings

L. Pezzato[a,*], M. Dabalà[a], Silvia Gross[b], K. Brunelli[a]

[a] Department of Industrial Engineering, University of Padova, Via Marzolo 9, 35131 Padova, Italy
[b] Department of Chemistry, University of Padova, Via Marzolo 1, 35131 Padova, Italy

ARTICLE INFO

Keywords:
Plasma electrolytic oxidation
PEO
Additive manufacturing
SLM
AlSi10Mg
Aluminum alloy
Corrosion

ABSTRACT

In this work, PEO process was carried out on SLM samples of AlSi10Mg, characterized by different grades of porosity, in direct-current mode using high current densities and short time in a basic silicate electrolyte. For comparison, the PEO process was also performed on samples of conventional cast AlSi10Mg alloy. The microstructure and the composition of the coatings was evaluated with SEM and XPS, whereas the phase analysis was performed with XRD. The corrosion resistance was analyzed by potentiodynamic polarization (PDP) and electrochemical impedance spectroscopy (EIS) tests.

The parameters used for PEO process allowed to obtain a continuous coating on all SLM samples, but its morphology resulted strongly influenced by the initial microstructure of the substrate. The coatings more homogeneous and less porous were produced on the samples with initial lower porosity. The corrosion performances of all SLM samples improved after PEO treatment and the PEO coatings with lower porosity resulted the more corrosion resistant.

1. Introduction

Industry is now benefiting from fabricating geometrically complex structures using a range of available additive manufacturing (AM) technologies. These processes have the potential to fulfil demands for reducing design to-manufacture time through replacing a series of production processes by a single-step process [1]. Among the AM methods, laser-based AM shows a very high potential for producing fully dense metallic structures using a variety of available metal powders and has attracted more and more attention [2]. Selective laser melting (SLM) is a process that uses high intensity laser as an energy source to directly fuse the metallic powder layers successively deposited one over the other as ultrathin two-dimensional cross-sections [3]. Among Al alloys, AlSi10Mg is the most applied for additive manufacturing (AM) processing studies, due to its attractive combination of mechanical properties, high heat conductivity and low weight, for application in automotive and aerospace [4].

Clearly the corrosion properties play a key role in the industrial application of AM objects and, from the literature, the comparison of corrosion properties of AM and cast samples of aluminum alloy still represents an open question. Some research found improved corrosion properties of AM samples, due to the homogenous microstructure and the absence of iron-based intermetallic [5,6], whereas other studies showed a decrease in the corrosion performances due to the reduced protection of the passive layer [7,8]. Despite the large interests and investigations about AM Al alloy samples and their corrosion properties, there is a lack of data showing protection methods against corrosion. Therefore, the aim of this work is to study a specific surface treatment to increase the corrosion resistance of SLM AlSi10Mg.

The most common surface treatment for aluminum alloys is anodizing but in literature was found that the anodizing process of AM aluminum alloys is characterized by slower kinetics than those of the cast alloy material and the oxide layer was generally thinner in the AM samples compared to the cast alloy [9]. To overcome the problems in anodizing AM Al–Si samples, due to the porosity and inhomogeneity in the microstructure, Plasma Electrolytic Oxidation (PEO) treatments can be tested. Among the surface treatments for Al alloys, PEO process seems to be one of the more promising due to the environmentally friendly nature of the electrolyte and due to the good properties of the obtained coatings [10]. Due to the high voltage, which is above the dielectric breakdown potential of the oxide layer, persistent anodic micro-discharges are formed on the surface during the PEO treatment

* Corresponding author at: Via Marzolo 9, 35131 Padova, Italy.
E-mail address: luca.pezzato@unipd.it (L. Pezzato).

https://doi.org/10.1016/j.surfcoat.2020.126477
Received 27 July 2020; Received in revised form 24 September 2020; Accepted 4 October 2020
Available online 07 October 2020
0257-8972/

and produce the growth of a protective ceramic coating [11]. PEO coatings are generally porous [12] and can be proper functionalized in order to give to the sample's particular properties [13]. Moreover, Snizhko et al. [14] and Sabatini et al. [15] showed that the presence of irregularity on the surface (shapes with complex geometries and non-line-of-sight areas) and the presence of Si precipitates, less affected the growth of the PEO coating in cast Al Alloys, in comparison with anodizing.

The production of PEO coatings on traditional aluminum alloys has been extensively studied in literature [16–18]. However, it has to be considered that the microstructure of the samples obtained with AM techniques is usually totally different from the one obtained on samples obtained with conventional manufacturing processes (silicon is uniformly distributed forming a cellular substructure inside of the melting pools, Fe and Mn intermetallic are totally absent) and this can produce significant differences during coating process [19,20]. Moreover, the presence of the porosity could influence the growth of the oxide layer. The use of PEO for AM aluminum alloys represents an innovation. In fact, only few works regarding the PEO treatment on AM Ti and Mg alloys for biomedical applications can be found in literature [21–24]. Regarding the application on Al alloys only one very recent work [25] can be found, but regard alternate current (AC) PEO treatment and do not focus on the corrosion properties of the sample, whereas about corrosion only one preliminary work of the authors can be found [26].

The aim of this work is so to produce by SLM samples of AlSi10Mg with a wide porosity range, and to use these samples as substrate for PEO process, in order to investigate the capability of PEO to protect against corrosion SLM samples of AlSi10Mg. The results will be compared with the ones of samples of AlSi10Mg produced by conventional casting process in order to study the influence of the microstructure on the final PEO coating.

2. Experimental

2.1. Production and characterization of SLM samples with different porosity

SLM AlSi10Mg alloy samples of 3 × 2 × 0.2 cm were employed as substrate for PEO coatings. The additive manufactured samples, obtained by Selective Laser Melting (SLM) were printed with a Renishaw AM400. The employed powders (provided by Renishaw, lot number UK3402) were obtained by gas-atomization and have an average grain size of 40 μm. The printing parameters are summarized in Table 1 and were chosen in order to obtain samples with different grades of porosity. In detail, four different SLM samples were produced and coated with PEO. Also, a conventional cast sample of AlSi10Mg was used for comparison.

The surface roughness was evaluated for the different SLM samples with a portable roughness meter ARW-100 with a 2.5 mm cut off and a total length of the measure of 12.5 mm. The parameters were chosen in order to evaluate only the roughness of the surface not considering the different porosity of the samples.

The microstructure of the AM samples was evaluated with a LEICA DMRE optical microscope (OM) and a Cambridge Stereoscan 440 scanning electron microscope (SEM), equipped with a Philips PV9800 EDS. The samples were polished with standard metallographic techniques (grinded until 4000 grit and polished with clothes with diamond suspension 6 and 1 μm) and analyzed to determine the porosity with image analysis using ImageJ software. To evaluate the microstructural features the samples were also etched with Graff-Sargent etch (84 ml water, 15.5 ml HNO_3, 0.5 ml HF, 3 g CrO_3). To evaluate the porosity, 10 images for each sample were employed in order to obtain representative results. Also, the cast sample was observed for comparison. EDS elemental maps were performed on both SLM and cast substrates in order to completely characterize the microstructure and the elemental distribution.

Table 1
Parameters for the production of SLM samples.

	Laser power (W)	Exposure time (ms)	Point distance (μm)	Hatch distance (μm)	Layer thickness (μm)
Sample 1	220	50	80	80	30
Sample 2	300	20	80	80	30
Sample 3	200	30	80	80	30
Sample 4	200	20	80	80	30

2.2. Production and characterization of PEO coatings

Before the PEO treatment the samples were degreased in acetone using ultrasounds and then dried with compressed air, without altering the initial surface. PEO process was performed in Direct Current (DC) mode employing a TDK-Lambda 350 V/8A power supply, with the sample that worked as anode and a carbon steel mesh that worked as cathode. An aqueous alkaline solution 25 g/l of Na_2SiO_3 and 2.5 g/l di NaOH was employed as electrolyte. The treatments were performed at 0.5 A/cm^2 for 10 min. During PEO process the temperature of the bath was maintained at 20 °C with a thermostatic bath. Both composition of the electrolyte and electrical parameters were chosen on the basis of previous works of the authors [18]. After the PEO treatment, the samples were washed with distilled water and ethanol and dried with compressed air. Both cross section and surface of the coated samples were analyzed at SEM-EDS to evaluate the morphological features, the homogeneity, the composition and the thickness of the coating. Also, EDS elemental maps were performed along the cross section to analyze the distribution of the elements into the coating. To analyze the cross section, the samples were cut with SiC disk, mounted in epoxy resin, grinded with abrasive papers until 4000 grit and polished with clothes and diamond suspension (6 μm and 1 μm). The phase composition of the PEO layers was evaluated by X-ray diffraction (XRD), performing Θ-2Θ scans from 10° to 90° with a 0.05 step size and a 1 s dwell time, by a Bruker D8 X-ray diffractometer with a Ni-filtered Cu-Kα radiation source (λ = 0.15405 nm), operating at 40 kV and 40 mA.

In order to deeply investigate the surface composition, the AlSi10Mg conventional cast sample and the SLM sample characterized by the lower porosity (SLM sample 1) were investigated by XPS measurements, with a Φ 5600ci Perkin-Elmer spectrometer, using a standard aluminum (Al Kα) source, with an energy of 1486.6 eV operating at 200 W. The X-ray source employed was located at 54.7° relative to the analyzer axis. The working pressure was < 5·10–8 Pa ~10–11 Torr. The calibration was based on the binding energy (B.E.) of the Au4f7/2 line at 83.9 eV with respect to the Fermi level. The standard deviation for the B.E. values was 0.15 eV. The reported B.E. were corrected for the B.E. charging effects, assigning the B.E. value of 284.6 eV to the C1s line of carbon. Survey scans were obtained in the 0–1350 eV. Detailed scans were recorded for relevant regions (O1s, C1s, Al2p, Si2p, Na1s, Al2s). The atomic composition, after a Shirley-type background subtraction, was evaluated using sensitivity factors supplied by Perkin-Elmer. The samples were loaded onto the XPS sample holder by using conducting biadhesive tape. The acquired data was then interpreted with the use of the Multipak software package. Assignment of the peaks was carried out according to literature data [27,28].

2.3. Corrosion resistance evaluation

The corrosion resistance of the samples was preliminary and qualitatively evaluated with potentiodynamic polarization tests (PDP) and then deeply analyzed with electrochemical impedance spectroscopy tests (EIS). Both PDP and EIS tests were performed in a 0.1 M Na_2SO_4 and 0.05 M NaCl solution to simulate a moderate aggressive environment containing both sulphates and chlorides. For each type of samples, three different samples were tested to assure reproducibility. PDP tests

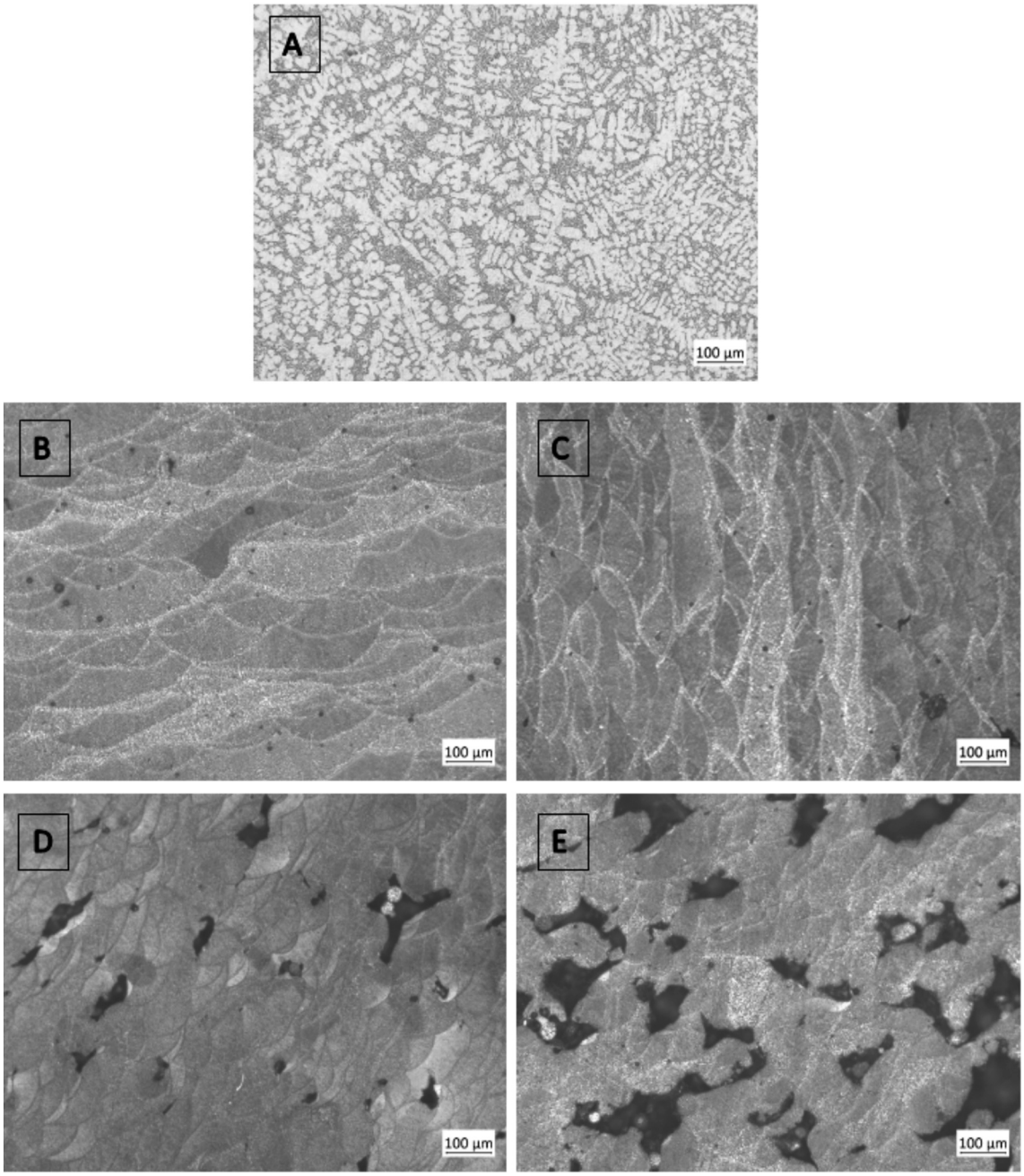

Fig. 1. Optical microscope (OM) images of the cast sample (A), sample 1 (B), sample 2 (C), sample 3 (D) and sample 4 (E) obtained at 100× with Graff-Sargent etch.

were carried out with and AMEL 2549 potentiostat using a saturated calomel electrode (SCE) as reference electrode and a Pt counter electrode. The potential scans were carried out after 30 min of open circuit voltage (OCP) stabilization, with a scan rate of 0.5 mV s-1 from −1.2 to −0.2 V. EIS tests were performed with the same cell employed for PDP at the value of the open circuit potential, after 1 h of stabilization, and in a frequency range between 10^5 Hz and 10^{-2} Hz, with a perturbation amplitude of 10 mV. The impedance measurements were recorded with a Materials Instrument Spectrometer coupled with the 2549 Potentiostat and the Z-View software was used for the fitting of impedance spectra. Both PDP and EIS tests were performed on coated and uncoated samples in order to understand, for the different manufacturing process and for the different porosity, the effect of the PEO treatment on the corrosion properties.

3. Results and discussion

3.1. Characterization of the substrates

The microstructure of SLM AlSi10Mg (Fig. 1b–e) exhibited significant differences with conventional cast one (Fig. 1a). In the conventional cast sample, the typical structure coming from solidification can be observed, with the presence of dendrites. Considering instead the SLM samples, the presence of laser tracks, accordingly to the building strategy, and of the melting pools, can be clearly observed. Inside the melting pools, a finer cellular microstructure can be noted. The microstructure resulted the typical one for aluminum alloys produced by SLM, as confirmed by literature [19,20]. As can be noted from Table 1 no differences in point distance, hatch distance and layer thickness were present on the samples and so, accordingly to this, no differences in the building structure were observed. The main

Table 2
Porosity and surface roughness of SLM samples, evaluated respectively with image analysis and with portable roughness meter.

	Porosity (%)	R_a (μm)
Sample 1/SLM	2.2 ± 0.5	19.1 ± 0.6
Sample 2/SLM	4.3 ± 0.4	20.0 ± 0.5
Sample 3/SLM	5.7 ± 0.8	19.5 ± 0.5
Sample 4/SLM	28.7 ± 1.5	19.7 ± 0.7

differences among the samples were related to the laser powder and the exposure time that cause a remarkable difference in the porosity, as can be observed both in Fig. 1 and Table 2.

In detail, the less porous sample (2.2% of porosity with image analysis) was the sample 1, obtained with intermediate laser power and long exposure time. The higher porosity (28.7%) was instead observed in the sample 4, produced with lower laser power and shorter exposure time. Sample 2 (high laser power and short exposure time) and sample 3 (low laser power and intermediate exposure time) showed intermediate porosity, 4.3% and 5.7%, respectively. The samples were specifically produced with different grades of porosity in order to analyze the effect of the pores on PEO coatings and their corrosion properties. Considering the surface roughness, in term of R_a, reported in Table 2, it can be observed that all the SLM samples were characterized by the same values of about 20 μm, indicating that the surface conditions of all the SLM samples were comparable and that the only difference in the samples was the porosity grade.

The BSE-SEM analysis of all SLM samples (Fig. 2a) showed a cellular structure, consisting of an interconnected Si network (lighter zone) dispersed within a α aluminum matrix. This microstructure, arising from the high cooling rates, is typical of the SLM process [19,20]. In Fig. 2a is reported the image of sample 1, considered as representative. Considering the structure of the conventional cast sample (Fig. 2b), are clearly visible the Si eutectic (in light grey) and of the Fe−Mn intermetallic (in white) in the Al matrix [6]. These considerations are confirmed also by EDS elemental maps, reported in Fig. 3. In the cast sample (Fig. 3a), the white particles resulted rich in Fe and Mn and the grey zones rich in Si, confirming the presence of the intermetallic and of the eutectic, respectively. In the sample 1 SLM (Fig. 3b) Si, Fe and Mn resulted dispersed in a homogeneous network.

3.2. Characterization of the PEO layers

The various samples, after PEO treatment, were characterized both on the surface and the cross section. The BSE-SEM observations are reported in Figs. 4–5, whereas the thickness of the different coatings is reported in Table 3. In the AlSi10 Mg conventional cast sample after PEO treatment (Fig. 4a) the coating was adherent to the substrate but with significant variations in the thickness that resulted around 40 μm but very uneven. The SEM analysis of the surface (Fig. 4b) evidenced the typical volcano-like pores [29]. A high number of large pores can be noted in fact on the surface. Moreover, the presence of a lot of pancake structures can be observed making the surface not smooth.

Considering the SLM sample 1 after PEO treatment (Fig. 5a, b), that is the one with the lowest porosity, a thicker layer (about 80 μm) adherent to the substrate can be observed. The surface morphology analysis (Fig. 5b) evidenced the presence of low number of volcano-pores with a quite smooth surface. The SLM sample 2 showed a similar surface morphology (Fig. 5d), with a reduced number of pores. Considering the cross section of sample 2 (Fig. 5c), the coating resulted adherent to the substrate and uniform but the thickness (54 μm) resulted reduced in comparison with sample 1. Considering SLM sample 3 and sample 4, that are the ones with the higher value of porosity, the observation of the surfaces (Fig. 5f and h, respectively) showed a high number of pores and pancake structures on the PEO layer, on the contrary of what observed for sample 1 and sample 2. The surfaces of samples 3 and 4 resulted similar to the one obtained on the cast one. Considering the cross sections of these samples, although the high grade of porosity, the coating resulted always adherent to the substrate. As a matter fact, also on sample 4, that is with 28.7% of porosity, the protective layer covered all the surface and, in case of porosities or irregular zones on the surface, these resulted “filled” by the protective oxide film. The thickness of the protective layer resulted about 75 μm for the sample 3 and 47 μm for sample 4.

Summarizing the SEM analysis of PEO layers formed on SLM samples with different porosity, an increase in the porosity of the coating was recorded when the porosity of the substrate was higher. This agrees with literature about the influence of the surface roughness on the morphology of PEO coatings. Zhu et al. [30] found that, on Ti6Al4V alloy, the PEO coating formed on the polished sample was less porous that the one obtained on sample grinded with 320 paper. Yoo et al. [31] reported similar results on AZ91 magnesium alloy, with a remarkable decrease in the porosity of the coating passing, for the substrate, from R_a = 2.5 μm to R_a = 0.5. Accordingly, to Zhu et al. [30] this fact is correlated with the radius of the spherical cavity where heterogeneous nucleation of the bubbles occurs during PEO process. This radius is linked with the surface roughness and resulted higher in the presence of higher surface roughness, thus producing larger bubbles. As cavities are formed due to bubbles break down, it is reasonable that higher surface roughness, or higher porosity of the substrate, produced more porous PEO coatings.

Comparing the coatings formed on SLM and on conventional cast sample, it can be observed that the coatings formed on SLM samples with low porosity are characterized by smoother and less porous surface than the one obtained on the cast sample. This fact can be explained with the microstructure of the substrate: in SLM samples the Fe-containing intermetallic were not present and the Si network was more dispersed than in the conventional cast alloy. As a matter of fact, Wu

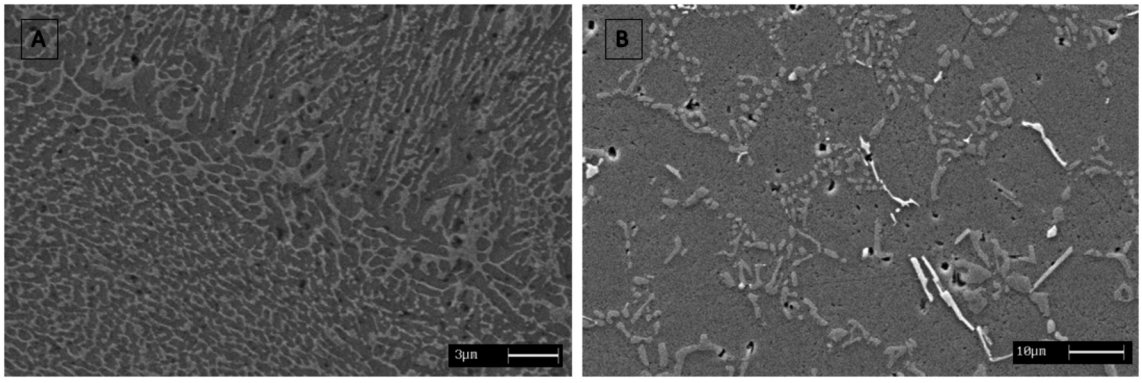

Fig. 2. BSE-SEM images of the sample 1 obtained with SLM (A) and of the conventional cast sample (B).

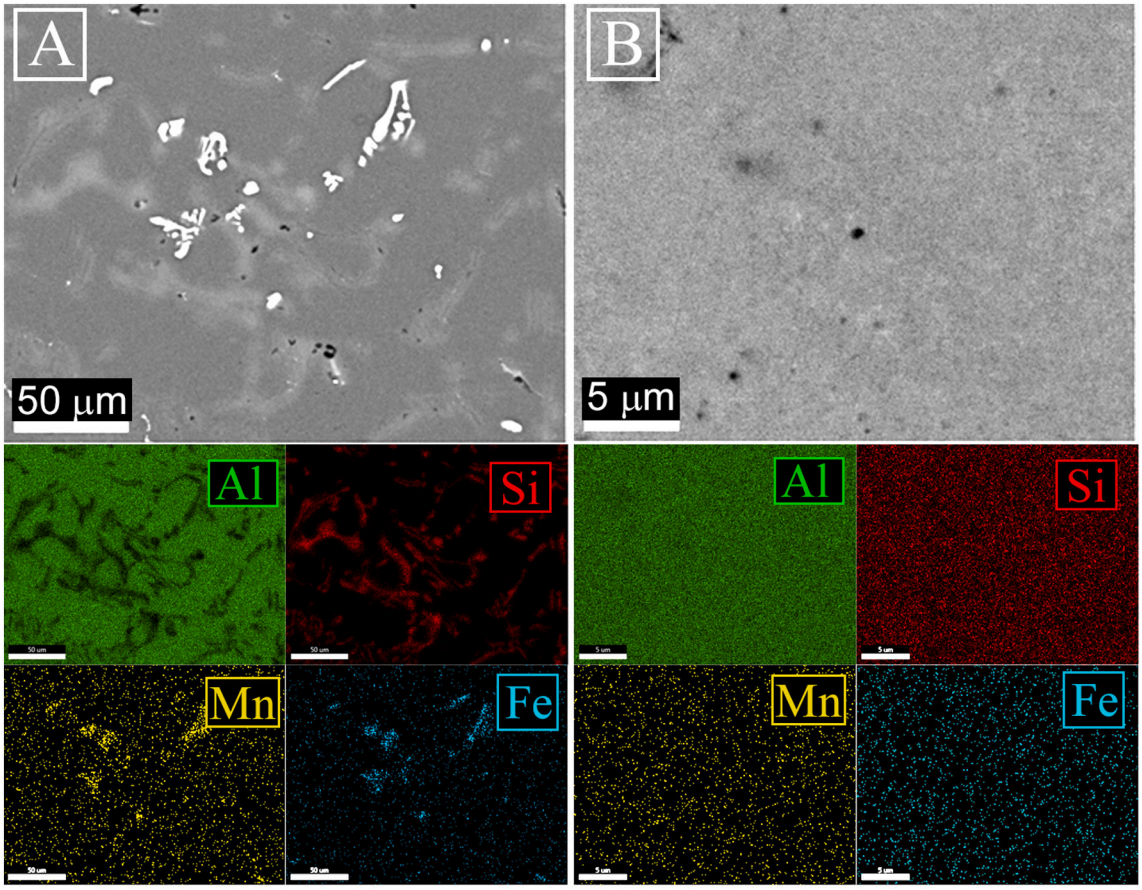

Fig. 3. EDS elemental map of the conventional cast sample (A) and of the sample 1 SLM (B). microstructures appeared less clear of the ones in Fig. 2 due to the fact that the samples are unetched.

et al. [32] found that the morphology of the PEO coatings on AlSi9Cu3 alloy was affected by the phases of the substrate, due to the different electrochemical behavior of the phases. In detail, they observed large micro pores on Fe-containing intermetallic and small micro-pores on eutectic Si. Moreover, the kinetic of the oxide growth was also found to depend on the phases of the substrate [32], thus explaining the heterogeneous thickness of the coating in the cast sample.

When the SLM substrates are very porous, the effect porosity overcame the one of the microstructures (samples 3 and 4).

The composition of the different PEO layers was investigated by SEM-EDS analysis. The results of the semi-quantitative EDS, performed both on the surface and on the cross section of the samples, are reported in Table 4. All the coatings resulted mainly composed by O, Si, Al, Na and Mg, in agreement with the composition of the electrolyte and of the substrate. The composition of all the SLM samples resulted similar and not dependent by the porosity. Comparing the SLM samples with conventional cast one, in this last sample the aluminum amount resulted higher and the silicon one lower. This fact can be correlated with the more homogeneous distribution of silicon in the SLM samples that allowed a better oxidation also of this element.

In order to study more deeply the distribution of the elements in the protective oxide coating, also EDS elemental mapping were performed along the cross section of the PEO coated conventional cast sample and 1 SLM sample (Fig. 6). Considering the coating on the cast sample

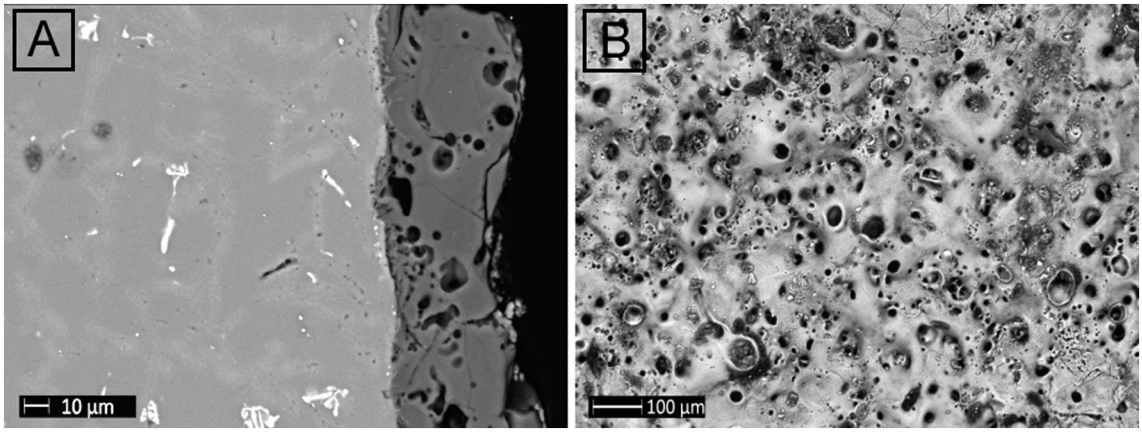

Fig. 4. SEM images of the PEO layers obtained on the conventional cast AlSi10Mg: cross section (A) and surface (B).

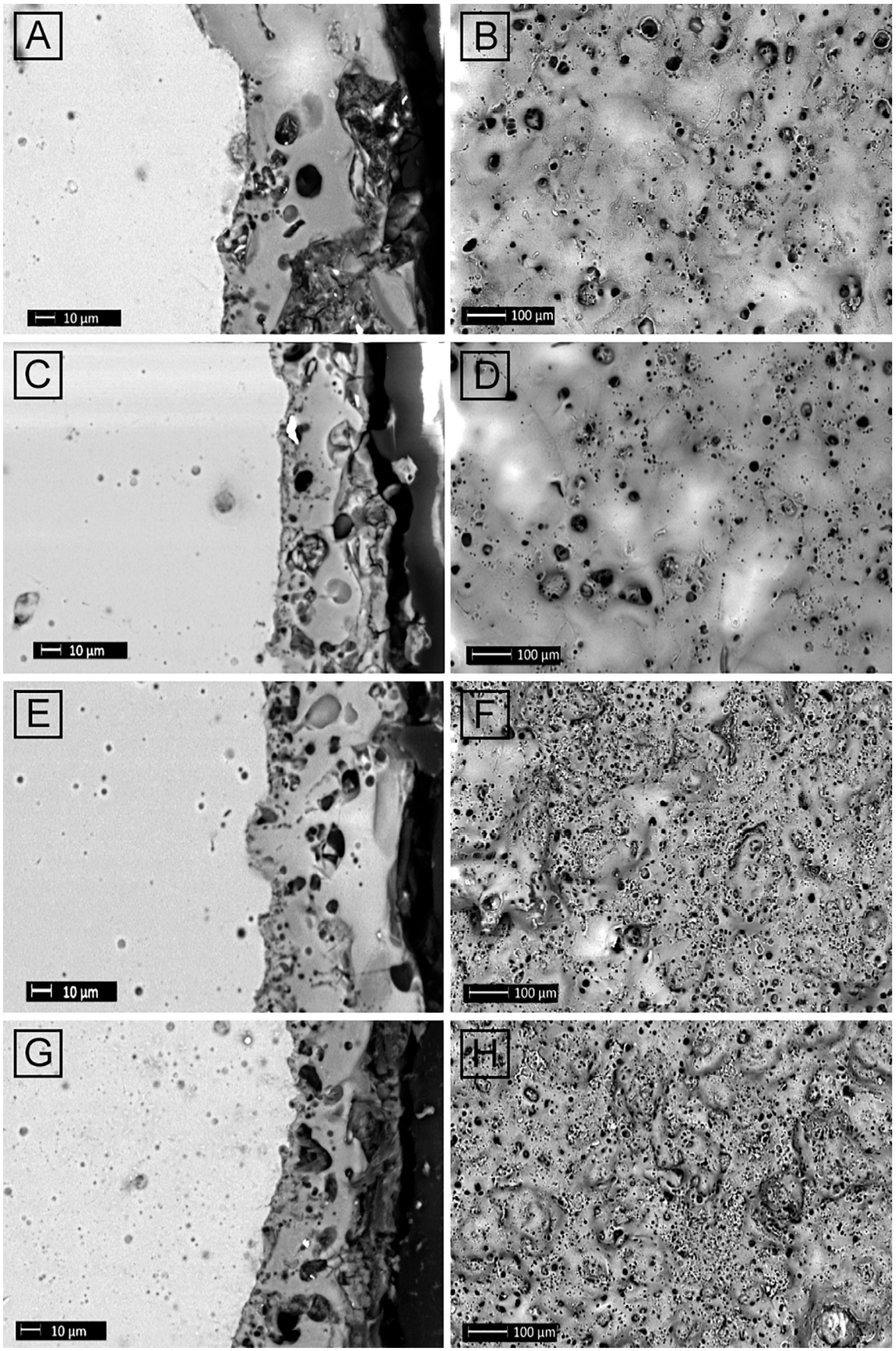

Fig. 5. SEM images of the PEO layers obtained on the SLM AlSi10Mg sample 1 (cross section (A) and surface (B)), sample 2 (cross section (C) and surface (D)), sample 3 (cross section (E) and surface (F)) and sample 4 (cross section (G) and surface (H)).

Table 3
Thickness of the PEO layers on the various samples evaluated from SEM observation.

PEO treated sample	Coating thickness (μm)
Sample 1/SLM	80 ± 20
Sample 2/SLM	54 ± 12
Sample 3/SLM	75 ± 12
Sample 4/SLM	47 ± 12
Cast AlSi10Mg	40 ± 25

Table 4
Results of the Semi-quantitative EDS analysis performed on the surface and the cross section of the various samples.

	Al%	O%	Na%	Si%	Mg%
Sample 1/SLM cross section	9.5	49.1	5.8	34.9	0.7
Sample 1/SLM surface	14.9	48.4	3.8	32.5	0.4
Sample 2/SLM cross section	10.3	49.1	3.8	36.0	0.8
Sample 2/SLM surface	14.9	49.3	2.1	33.3	0.4
Sample 3/SLM cross section	6.3	54.8	–	38.3	0.6
Sample 3/SLM surface	12.2	49.7	3.2	34.4	0.5
Sample 4/SLM cross section	8.8	48.1	12.1	30.4	0.6
Sample 4/SLM surface	12.9	51.3	2.9	33.5	0.4
Cast AlSi10Mg cross section	22.9	47.7	–	28.9	0.5
Cast AlSi10Mg surface	10.7	48.2	8.7	32.0	0.4

(Fig. 6a) a non-uniform distribution of the different elements along the coating can be observed. This fact resulted in accordance with the literature on PEO coatings. Krishtal et al. [33] found in fact that an inhomogeneous distribution of silicon in a silumin substrate produced a non-uniform distribution of silicon in the PEO layer. In the cast alloy silicon is concentrated in the eutectic zones ad near these zones an enrichment in silicon in the coating can be observed. Moreover, Dehnavi et al. [34] evidenced that an increase in the duty cycle produce a non-uniform distribution of Si into the coating; the DC mode can be considered as working with 100% of duty cycle and so this fact can further increase the inhomogeneity of the PEO layer. From the analysis of the maps performed on PEO coated 1 SLM sample (Fig. 6b) a more uniform distribution of Si and of the other elements can be observed into the coating, probably due to the more homogenous distribution of the elements in the substrate, as evidenced in Fig. 3b.

To evaluate the phase composition of the coatings, XRD analysis were performed and the results are reported in Fig. 7. Considering that the patterns of the SLM samples were very similar, only the one of sample 1 is reported (Fig. 7a), and compared with the one of the cast sample (Fig. 7b).

In both the samples, the peaks of Al and Si, coming from the reflection from the substrate, can be observed. In both the samples were found also the peaks of SiO_2, Al_2O_3 Al_2SiO_5 (kyanite), in agreement with literature [35], and of $NaAlSi_3O_8$. However, the main difference in the two patterns was the amount of amorphous phase, which resulted remarkably higher in SLM sample. This fact is agreement with the only work, which was recently published on PEO coatings on AM aluminum alloys [25]. Although the subject is new and still under investigation, Rogov et al. explained this behavior with the more homogeneous microstructure of the 3D printed alloy that promotes a simultaneous oxidation of Al and Si rich micro-regions, resulting in a mixture of small X-ray amorphous crystals [25].

In order to have information also on the more external layer of the PEO coating, XPS analysis were performed on the SLM sample 1 and on the conventional cast sample. The results of the survey scans and of the quantitative analysis are reported in Fig. 8 and Table 5. The two samples are very similar in term of composition: O, Si, Al, Na and Mg were detected. The presence of C was due to contamination.

The XPS high resolution spectra of the SLM sample 1 after PEO treatment are shown in Fig. 9a–d. The oxygen spectrum was deconvoluted in three main components: the main peak located at 531.8 eV BE corresponding to the metal hydroxides and to alumina silicate compounds, whereas the peak at 532.7 eV and at 530 eV BE was attributed to silicate compounds and metal oxides, respectively [36] (Fig. 9a). The high-resolution Al2p peak is shown in Fig. 9b, where the peak at 74.2 eV BE is consistent with aluminosilicate, whereas the peak located at 73.5 eV BE corresponds to Al_2O_3.

The high resolution Si2p peak is reported in Fig. 9c, and the peak at 102.2 eV BE was attributed to silicate compounds, whereas the other one located at 102.7 is consistent with the presence of aluminosilicate compounds [36].

The peak of Na 1s at 1071.70 eV BE was attributed to (SiO_2) 0.7(Na_2O)0.3 [17], whereas the peak at 1072. 2 is compatible with the presence of $NaAlSi_3O_8$ [28].

The XPS high resolution spectra of the conventional cast sample after PEO treatment are shown in Fig. 9e–h, and the results are similar to those found for SLM sample 1.

Summarizing, the surface of both the samples was constituted mainly by alumina silicate compounds, silicate compounds and Al_2O_3.

3.3. Corrosion properties

The corrosion resistance of the different samples was evaluated with PDP and EIS tests. Potentiodynamic polarization tests were performed only for a qualitative and comparative analysis, due to the fact that no quantitative evaluation on the corrosion rate can be performed on samples coated with a thick insulating film, due to the fact that the Tafel law cannot be applied [37]. Considering this, corrosion potentials and corrosion current densities were calculated only for some selected untreated samples. For each sample only one of the three measured Tafel curves is presented, for clarity reasons (the three curves where comparable with low statistical error). EIS tests were performed to obtain quantitative data on the corrosion resistance of the different samples.

In Fig. 10 are reported the PDP curves of the SLM sample 1 and of the conventional cast sample before and after the PEO treatment, in order to compare the behavior of the SLM sample with the cast one. Considering the untreated samples, a slight increase in the corrosion properties of the SLM sample 1 ($E_{corr} = -0.88 \pm 0.05$ V, $i_{corr} = 7.0 \pm 1 \times 10^{-7}$ A/cm^2) in comparison with the cast one ($E_{corr} = -0.90 \pm 0.06$ V, $i_{corr} = 7.0 \pm 1.1 \times 10^{-6}$ A/cm^2) can be noticed. In particular, the corrosion potential remained the same in the two samples, whereas a decrease of one order on magnitude in the corrosion current was observed in the SLM sample 1, in comparison with the conventional cast one. On cast samples the corrosion starts preferentially near the Fe-containing intermetallic and the Si-eutectic, as evidenced by Arrabal et al. [38]. In the AM samples the corrosion instead proceeds by selective dissolution of the α-Al phase along the edges of melt pools, due to the presence of more noble precipitates of silicon, as stated by Cabrini et al. [8]. Generally, the corrosion resistance of AM samples is slightly higher than the cast one, due to the absence of Fe-containing intermetallic, the fine grain size, the absence of impurities and the uniform distribution of Si that prevent galvanic corrosion as stated by Leon et al. and Fathi et al. [5,6].

Considering the PEO treated samples, in both cases the treatment increased significantly the corrosion properties of the AlSi10Mg alloy, indicating that the treatment was effective both on samples produced with traditional casting and additive manufacturing. For the PEO treated samples the slight increase in the corrosion properties of the SLM sample in comparison with the cast one was maintained. This fact can be linked with the microstructural observation above reported, in fact the PEO layer obtained on SLM sample 1 was less porous and thicker than the one obtained on the cast sample.

In order to understand the influence of the porosity on the corrosion properties of the samples, in Fig. 11 are reported the PDP curves of all the untreated and PEO treated SLM samples. First of all, can be noticed

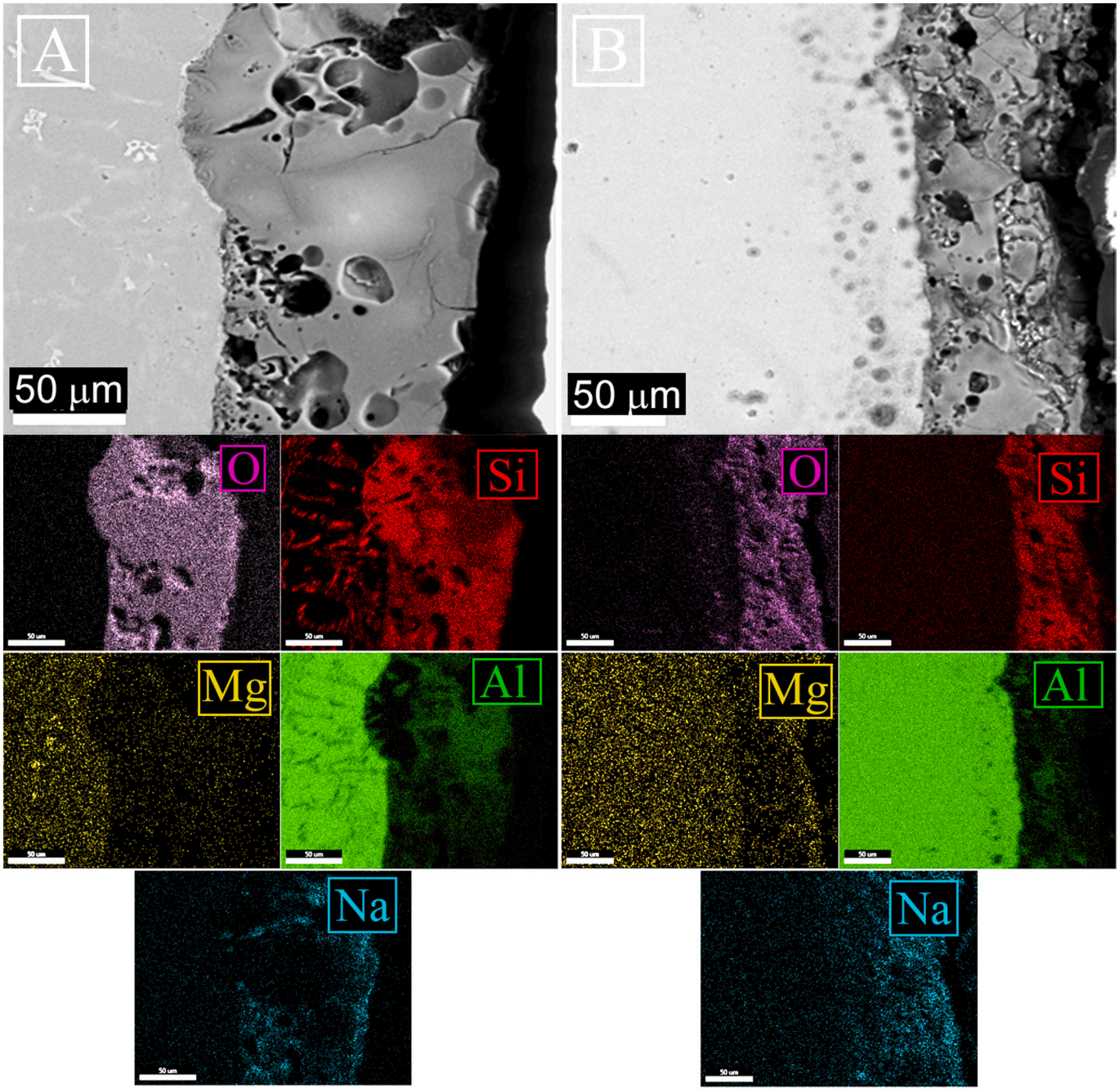

Fig. 6. EDS elemental mapping performed on the cross sections of the PEO treated cast sample (A) and of the PEO treated sample 1 SLM (B).

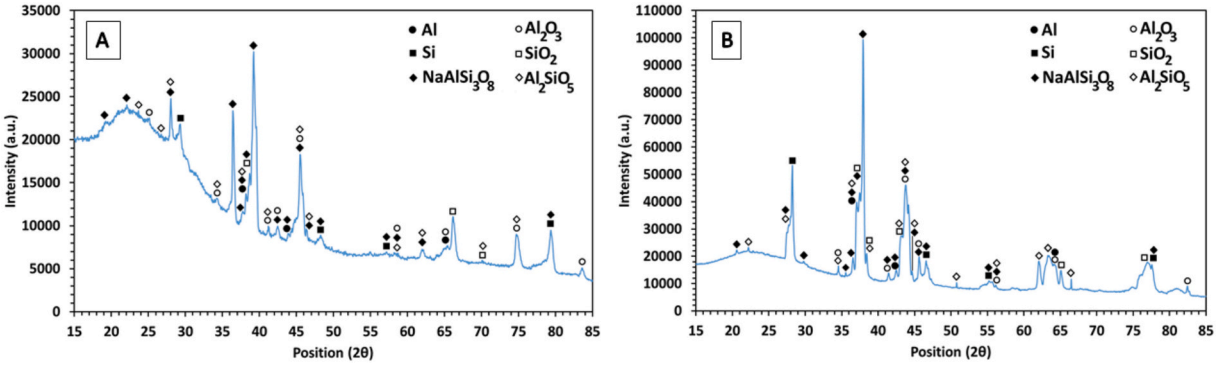

Fig. 7. XRD pattern of the SLM sample 1 (A) and of the AlSi10Mg conventional cast sample (B).

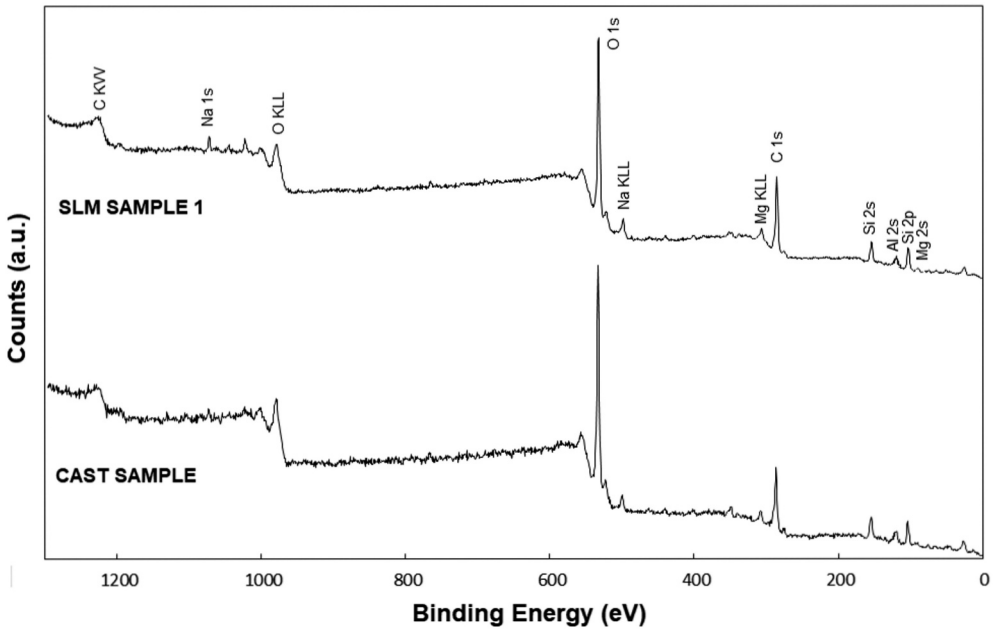

Fig. 8. Survey scans collected from the samples: Sample 1/SLM and AlSi10Mg cast with main peaks indexed. Binding energies not corrected for surface charging. Minor and less visible peaks were not indexed.

Table 5
Surface composition (atomic %) of the SLM "Sample 1" and of the AlSi10Mg cast sample.

Sample	C%	O%	Al%	Na%	Mg%	Si%
Sample 1/SLM	42.1	38.0	4.6	2.1	2.2	11.0
AlSi10Mg Cast	34.7	45.4	4.5	1.7	1.8	11.9

that, regardless the porosity, the PEO treatment resulted effective in increasing the corrosion resistance of the samples. In fact, from the sample 1 (2.2% of porosity) to the sample 4 (28.7% of porosity) a remarkable shift towards smaller currents and higher potentials can be observed. Analyzing the behavior of the uncoated samples, the porosity resulted detrimental for the corrosion properties, in agreement with Kong et al. [39] that found localized corrosion inside the pores due to different aeration.

The sample 4 resulted in fact the worst in term of corrosion properties, whereas the others (samples 1, 2, 3) showed comparable corrosion resistance. Considering the PEO treated samples, sample 1 and sample 2 showed better corrosion properties than sample 3 and sample 4. In fact, a clear shift towards more cathodic currents can be observed. This fact agrees with the microstructure of the PEO layers: sample 1 and sample 2 were characterized by a smooth surface with reduced number of pores, whereas sample 3 and sample 4 presented surfaces with large number of pores and pancake structures. Thus, the increase in the porosity of the protective coating resulted detrimental for the corrosion resistance.

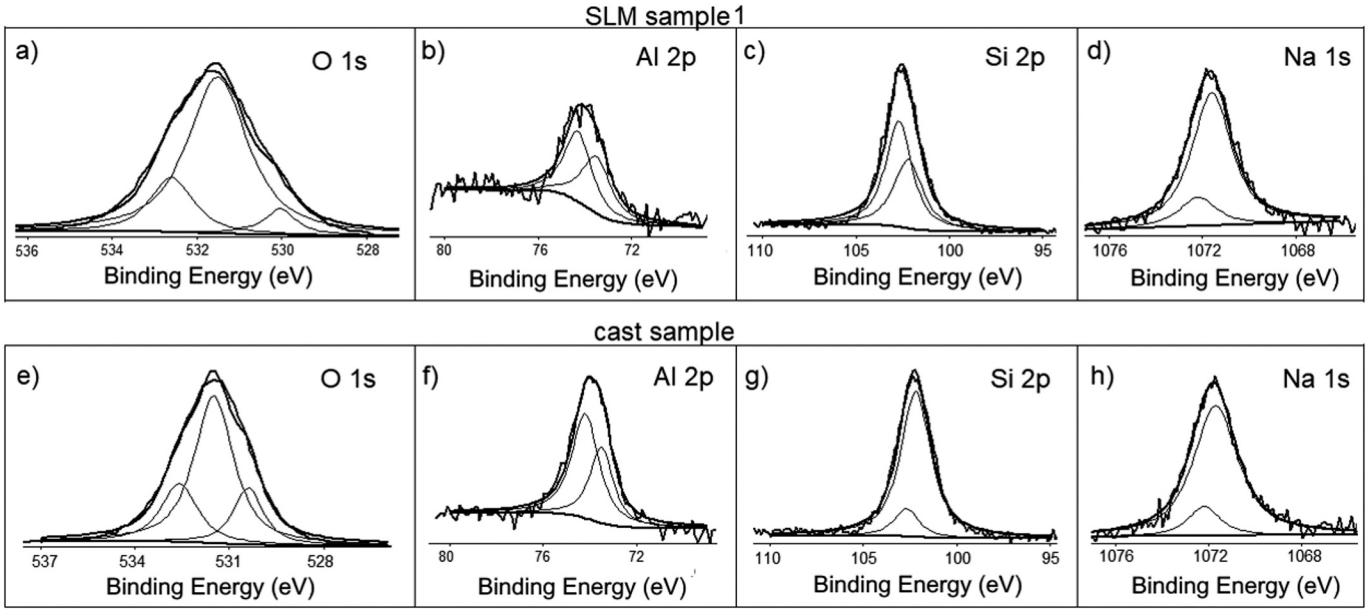

Fig. 9. High resolution single peak spectra of the O1s region ((a) Sample1/SLM, (e) cast sample), the Al2p region ((b) Sample1/SLM, (f) cast sample), the Si2p region ((c) Sample1/SLM, (g) cast sample) and Na1s region ((d) Sample1/SLM, (h) cast sample).

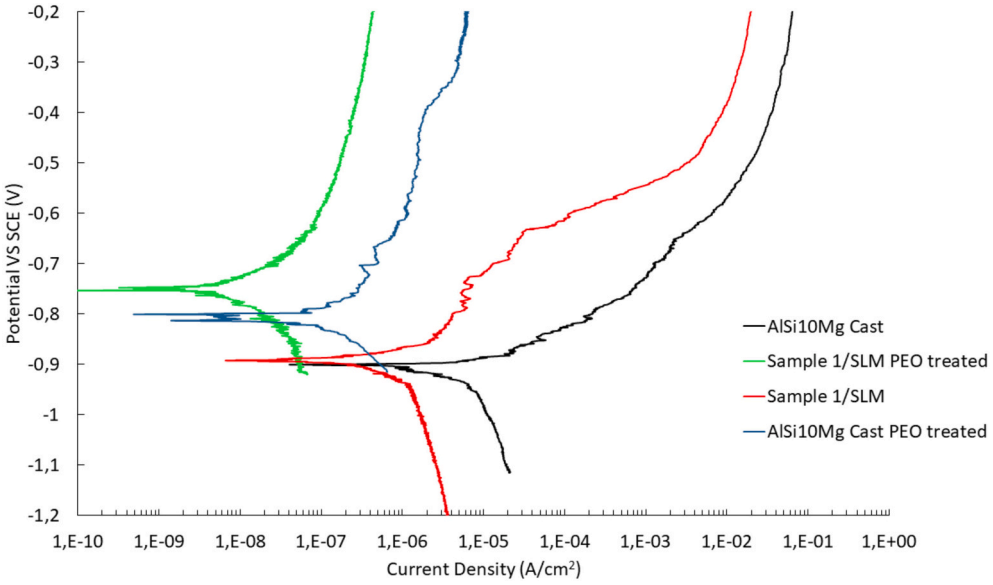

Fig. 10. Results of potentiodynamic polarization tests performed on the AlSi10Mg cast sample and on the Sample 1/SLM before and after PEO treatment (Test Electrolyte: 0.1 M Na_2SO_4 and 0.05 M NaCl).

In order to deeply study the corrosion behavior of the various samples, electrochemical impedance spectroscopy (EIS) tests were performed. The fitting of the experimental data was performed with Z-view software, using the equivalent circuits reported in Fig. 12. Two different equivalent circuits were employed to consider both untreated and PEO treated samples. For the untreated samples a simple R/CPE circuit was employed as only natural oxide layer is present (Fig. 12a), whereas the equivalent circuit of Fig. 12b was used for PEO treated samples, in agreement with literature data [40]. This double circuit is employed in PEO coated samples in order to consider the presence of two layers: an external porous layer and an internal barrier layer.

Considering the meaning of the different electrical elements R_e represents the resistance of the electrolyte, R_p the polarization resistance of the porous layer and R_b the polarization resistance of the barrier layer. In the untreated sample the polarization resistance of the natural oxide layer is called R_o. CPE_i were used in the equivalent circuit instead of capacitances due to the fact that the measured capacitance is not ideal.

The EIS results of the SLM and the conventional cast samples, in term of Nyquist plot, are shown in Fig. 13; the results for the untreated samples are reported in Fig. 13a, whereas the ones for the PEO treated samples in Fig. 13b. The results of the fitting of the experimental data are presented in Table 6. First of all, can be noticed the good quality of the fitting with the good correspondence between dots and lines in the Nyquist plots and the low values of chi-squared.

From the analysis of the data, in all the cases the PEO treatment induced a remarkable increase in the corrosion properties, confirming the results coming from PDP. In fact, the untreated samples were characterized by polarization resistances from 80 to 160 $\Omega \cdot cm^2$, whereas the ones of PEO coated samples varied between 5000 and 9000 $\Omega \cdot cm^2$, with an increase of over one order of magnitude. These results demonstrated that, regardless the porosity, PEO treatment increased the corrosion properties of AlSi10Mg, and confirmed the high versatility of this treatment, in comparison with traditional treatments,

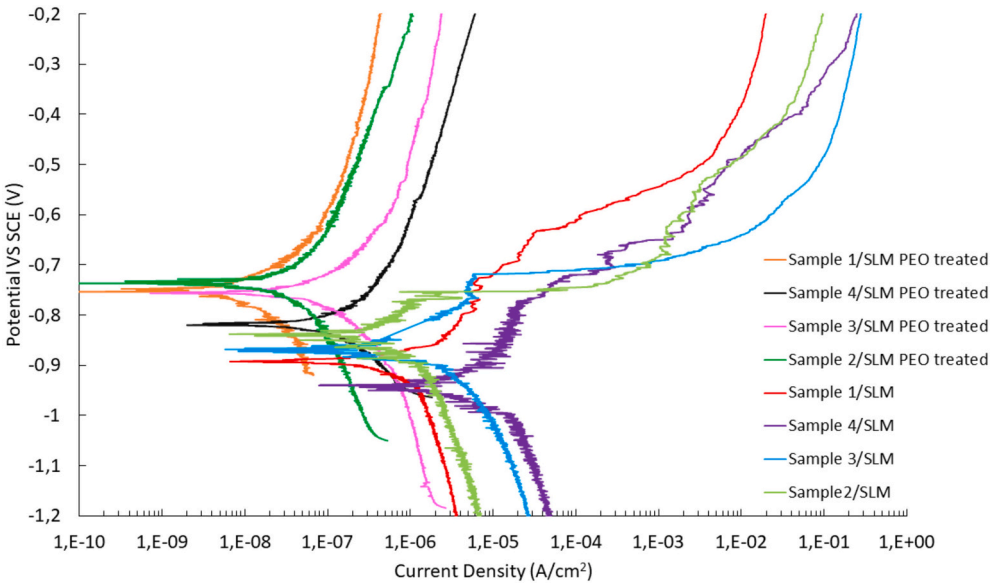

Fig. 11. Results of potentiodynamic polarization tests performed on the SLM samples with different porosity grades before and after PEO treatment (Test Electrolyte: 0.1 M Na_2SO_4 and 0.05 M NaCl).

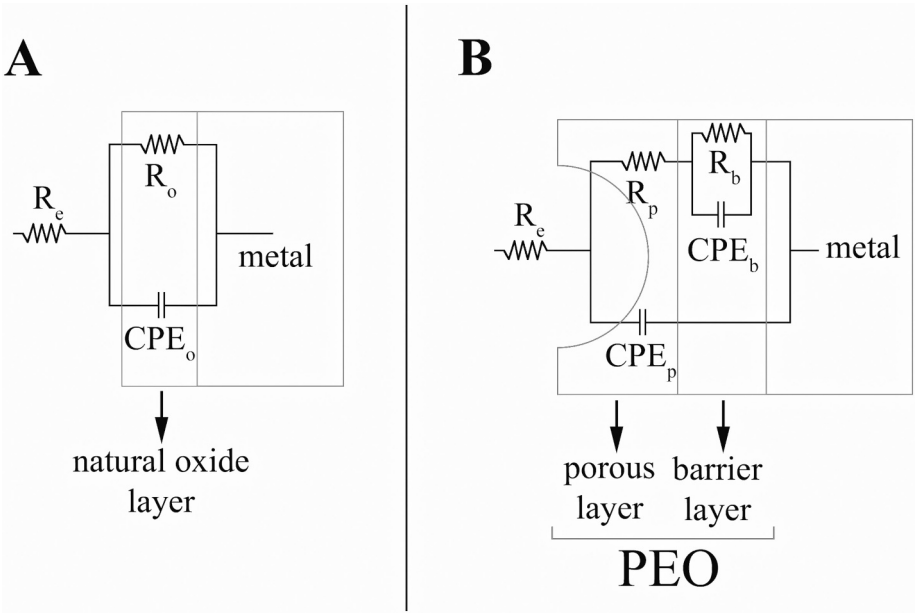

Fig. 12. Equivalent circuit employed in the fitting of the experimental data coming from EIS tests. The circuit in (A) was used for the untreated samples, whereas the circuit in (B) for the PEO treated samples.

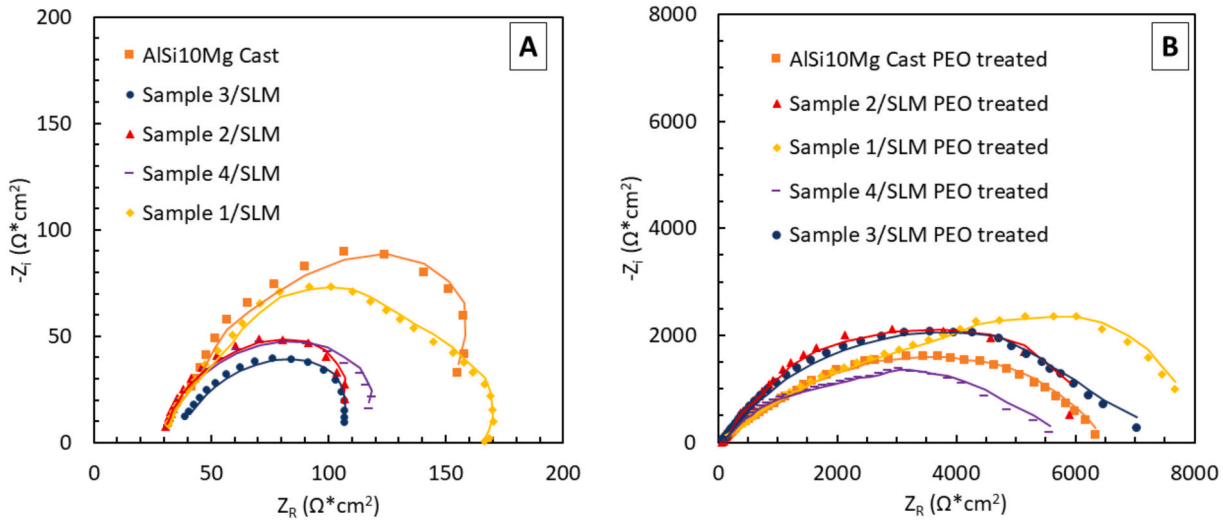

Fig. 13. Results of EIS tests in form of Nyquist plots for all the untreated samples (A) and all the PEO treated samples (B) Dots represent experimental data, lines the results of the fitting (Test Electrolyte: 0.1 M Na_2SO_4 and 0.05 M NaCl).

such as anodizing, that are not able to produce a protective layer on samples characterized by high porosity or high surface roughness, as described in literature by Menargues et al. [41] and Caliari et al. [42].

Considering the PEO treated samples (Fig. 13b), it can be noticed that the sample characterized by the higher corrosion properties (polarization resistance R_B over 8000 Ω·cm^2) is the sample 1/SLM. The sample with the lower corrosion properties is instead the sample 4/SLM (R_B of 5680 Ω·cm^2 after PEO treatment). These results are in accordance

Table 6
Results of the fitting of the experimental data coming from EIS tests.

Sample	R_S (Ω·cm^2)	R_o o R_P (Ω·cm^2)	R_B (Ω·cm^2)	Q_P (F·Hz^{1-n})	n_P	Q_B (F·Hz^{1-n})	n_B	χ^2
Sample 1/SLM	30	162.1	–	3.0×10^{-6}	0.75	–	–	8×10^{-3}
Sample 2/SLM	30	83.9	–	2.0×10^{-6}	1.0	–	–	7×10^{-3}
Sample 3/SLM	30	87.2	–	6.6×10^{-6}	0.85	–	–	7×10^{-3}
Sample 4/SLM	30	95.3	–	3.5×10^{-6}	0.95	–	–	2×10^{-3}
AlSi10Mg Cast	30	147.0	–	2.0×10^{-6}	0.96	–	–	2×10^{-2}
Sample 1/SLM PEO Treated	30	144.5	8391	4.5×10^{-8}	1.0	2.9×10^{-5}	0.53	1×10^{-4}
Sample 2/SLM PEO Treated	30	44.62	6158	3.6×10^{-6}	0.62	4.3×10^{-6}	0.65	1×10^{-1}
Sample 3/SLM PEO Treated	30	83.23	6824	3.2×10^{-6}	0.73	3.9×10^{-5}	0.69	6×10^{-5}
Sample 4/SLM PEO Treated	30	53.4	5688	8.6×10^{-5}	0.55	9.2×10^{-7}	0.98	6×10^{-3}
AlSi10Mg Cast PEO Treated	30	44.9	6244	1.2×10^{-6}	0.80	2.5×10^{-5}	0.60	7×10^{-4}

with the previously reported PDP results and with the morphology of the different PEO layers, with the coating produced on sample 1/SLM that is less porous and thicker than the one obtained on sample 4/SLM. All the other samples exhibit intermediate corrosion behavior with values of R_b between 6000 and 7000 Ω·cm^2. Generally, the behavior of all the PEO treated samples can be considered comparable, evidencing the capability of PEO process to successfully protect both cast and AM samples, regardless the porosity. The increased corrosion resistance given by PEO coatings on cast Al−Si alloys agreed with the results reported in literature. Mohedano et al. [43,44] found in fact for A356 alloy a remarkable improvement in the corrosion resistance after PEO treatment in comparison with conventional anodizing, thanks to the absence of secondary phases with different oxidation behavior. Also, Li et al. [45] obtained thick and homogenous PEO coatings on eutectic Al−Si alloy and found that the presence of 0.1% of Sr in the alloy allowed the growth of a thicker and denser film. The testing electrolyte employed in this work is different, however the recorded improvement in the corrosion behavior is comparable to the one found by Li et al. [45] and lower than the one observed by Mohedano et al. [43,44], probably due to higher porosity of the oxide film in this case. Considering the results on Al−Si SLM samples the improved corrosion performances after PEO treatment resulted in accordance with a preliminary work published by the authors on this subject [26].

4. Conclusions

PEO coatings were successfully produced both on cast and SLM samples with different porosity grades. The initial microstructure and porosity of the substrate influenced the morphology of the PEO layer that resulted smooth and less porous for the SLM samples with low porosity, whereas was very porous with a lot of pancake structures for the cast sample and for the SLM samples with higher porosity. From XRD analysis the coating resulted mainly composed by phases containing Al and Si, with a remarkable increase of the amorphous fraction in the SLM sample, if compared with the cast one. Considering the corrosion properties of the untreated samples, the sample that showed the best corrosion properties was the sample 1/SLM thank to the absence of Fe-containing intermetallic, the homogenous microstructure and the absence of pores. Considering the PEO coated samples, in all the cases a remarkable increase in the corrosion properties was recorded, evidencing the possibility to successfully coat samples with different microstructures and different porosity, on the contrary of what happens with more traditional techniques such as anodizing. The sample 1/SLM after PEO coating showed the higher corrosion resistance due to the smooth and less porous coating.

CRediT authorship contribution statement

L. Pezzato: Methodology, Software, Validation, Formal analysis, Investigation, Data curation, Writing - original draft, Writing - review & editing. **M. Dabalà:** Methodology, Visualization, Supervision. **S. Gross** Investigation, Formal analysis. **K. Brunelli:** Conceptualization, Resources, Writing - original draft, Writing - review & editing, Supervision, Project administration, Funding acquisition.

Declaration of competing interest

The authors declare that they have no known competing financial interests or personal relationships that could have appeared to influence the work reported in this paper.

Acknowledgements

This research was supported by Department of Industrial Engineering, University of Padua (BIRD 2018).

DiSC and ICMATE-CNR (Padova) is gratefully acknowledged for financial support and provision of XPS equipment.

The authors gratefully acknowledge also Tesolin S.p.A. for the production of SLM samples.

References

[1] N.T. Aboulkhair, M. Simonelli, L. Parry, I. Ashcroft, C. Tuck, R. Hague, 3D printing of aluminium alloys: additive manufacturing of aluminium alloys using selective laser melting, Prog. Mater. Sci. 106 (2019) 100578.
[2] A. Aversa, G. Marchese, A. Saboori, E. Bassini, D. Manfredi, S. Biamino, D. Ugues, P. Fino, M. Lombardi, New aluminum alloys specifically designed for laser powder bed fusion: a review, Materials 12 (2019) 1007.
[3] E.O. Olakanmi, R.F. Cochrane, K.W. Dalgarno, A review on selective laser sintering/melting (SLS/SLM) of aluminium alloy powders: processing, microstructure, and properties, Prog. Mater. Sci. 74 (2015) 401–477.
[4] J.H. Martin, B.D. Yahata, J.M. Hundley, J.A. Mayer, T.A. Schaedler, T.M. Pollock, 3D printing of high-strength aluminium alloys, Nature 549 (2017) 365–369.
[5] P. Fathi, M. Mohammadi, X. Duan, A.M. Nasiri, A comparative study on corrosion and microstructure of direct metal laser sintered AlSi10Mg_200C and die castA360.1 aluminum, J. Mater. Process. Technol. 259 (2018) 1–14.
[6] A. Leon, A. Shirizly, E. Aghion, Corrosion behavior of AlSi10Mg alloy produced by additive manufacturing (AM) vs. its counterpart gravity cast alloy, Metals 6 (7) (2016) 148.
[7] M. Cabrini, S. Lorenzi, T. Pastore, S. Pellegrini, D. Manfredi, P. Fino, S. Biamino, C. Badini, Evaluation of corrosion resistance of Al–10Si–Mg alloy obtained by means of Direct Metal Laser Sintering, J. Mater. Process. Technol. 231 (2016) 326–335.
[8] M. Cabrini, S. Lorenzi, T. Pastore, C. Testa, D. Manfredi, M. Lorusso, F. Calignano, M. Pavese, F. Andreatta, Corrosion behavior of AlSi10Mg alloy produced by laser powder bed fusion under chloride exposure, Corros. Sci. 152 (2019) 101–108.
[9] R.I. Revilla, D. Verkens, G. Couturiaux, L. Malet, L. Thijs, S. Godet, I. De Graeve, Galvanostatic anodizing of additive manufactured Al-Si10-Mg alloy, J. Electrochem. Soc. 164 (14) (2017) C1027–C1034.
[10] V. Dehnavi, B. Li Luan, X. Yang Liu, D.W. Shoesmith, S. Rohani, Correlation between plasma electrolytic oxidation treatment stages and coating microstructure on aluminum under unipolar pulsed DC mode, Surf. Coat. Technol. 269 (2015) 91–99.
[11] J. Martin, A. Melhem, I. Shchedrina, T. Duchanoy, A. Nominè, G. Henrion, T. Czerwiec, T. Belmonte, Effects of electrical parameters on plasma electrolytic oxidation of aluminium, Surf. Coat. Technol. 221 (2013) 70–76.
[12] J.A. Curran, T.W. Clyne, Porosity in plasma electrolytic oxide coatings, Acta Mater. 54 (2006) 1985–1993.
[13] L. Pezzato, P. Cerchier, K. Brunelli, A. Bartolozzi, R. Bertani, M. Dabalà, Plasma electrolytic oxidation coatings with fungicidal properties, Surf. Eng. 35 (2019) 325–333.
[14] L.O. Snizhko, A.L. Yerokhin, A. Pilkington, N.L. Gurevina, D.O. Misnyankin, A. Leyland, A. Matthews, Anodic processes in plasma electrolytic oxidation of aluminium in alkaline solutions, Electrochim. Acta 49 (2004) 2085–2095.
[15] G. Sabatini, L. Ceschini, C. Martini, J.A. Williams, I.M. Hutchings, Improving sliding and abrasive wear behaviour of cast A356 and wrought AA7075 aluminium alloys by plasma electrolytic oxidation, Mater. Des. 31 (2010) 816–828.
[16] X. Huang, L. Famiyeh, Plasma electrolytic oxidation coatings on aluminum alloys: microstructures, properties, and applications, Mod. Concept Mater. Sci. 2 (2019) (MCMS.MS.ID.000526).
[17] E. Matykina, R. Arrabal, M. Mohedano, B. Mingo, J. Gonzalez, A. Pardo, M.C. Merino, Recent advances in energy efficient PEO processing of aluminium alloys, Trans. Nonferrous Met. Soc. China (Eng. Ed.) 27 (2017) 1439–1454.
[18] P. Cerchier, L. Pezzato, C. Gennari, E. Moschin, I. Moro, M. Dabalà, PEO coating containing copper: a promising anticorrosive and antifouling coating for seawater application of AA 7075, Surf. Coat. Technol. 393 (2020) 125774.
[19] X. Liu, C. Zhao, X. Zhou, Z. Shen, W. Liu, Microstructure of selective laser melted AlSi10Mg alloy, Mater. Des. 168 (2019) 107677.
[20] F. Trevisan, F. Calignano, M. Lorusso, J. Pakkanen, A. Aversa, E.P. Ambrosio, M. Lombardi, P. Fino, D. Manfredi, On the selective laser melting (SLM) of the AlSi10Mg alloy: process, microstructure, and mechanical properties, Materials 10 (2017) 76.
[21] P. Xiu, Z. Jia, J. Lv, C. Yin, Y. Cheng, K. Zhang, C. Song, H. Leng, Y. Zheng, H. Cai, Z. Liu, Tailored surface treatment of 3D printed porous Ti6Al4V by microarc oxidation for enhanced osseointegration via optimized bone in-growth patterns and interlocked bone/implant interface, ACS Appl. Mater. Interfaces 8 (2016) 17964–17975.
[22] Z. Gorgin Karaji, R. Hedayati, B. Pouran, I. Apachitei, A.A. Zadpoor, Effects of plasma electrolytic oxidation process on the mechanical properties of additively manufactured porous biomaterials, Mater. Sci. Eng. C 76 (2017) 406–416.
[23] J. Chen, J. Li, F. Hu, Q. Zou, Q. Mei, S. Li, Y. Hao, W. Hou, J. Li, Y. Li, Y. Zuo, Effect of microarc oxidation-treated Ti6Al4V scaffold following low-intensity pulsed ultrasound stimulation on osteogenic cells in vitro, ACS Biomater. Sci. Eng. 5 (2019) 572–581.
[24] S.V. Gnedenkov, S.L. Sinebryukhov, V.S. Egorkin, D.V. Mashtalyar, I.E. Vyaliy, K.V. Nadaraia, I.M. Imshinetskiy, A.I. Nikitin, E.P. Subbotin, A.S. Gnedenkov, Magnesium fabricated using additive technology: specificity of corrosion and protection, J. Alloys Compd. 808 (2019) 151629.
[25] A.B. Rogov, H. Lyu, A. Matthews, A. Yerokhin, AC plasma electrolytic oxidation of additively manufactured and cast AlSi12 alloys, Surf. Coat. Technol. 126116 (2020)

(in press).
[26] L. Pezzato, M. Dabalà, K. Brunelli, Microstructure and corrosion properties of PEO coatings produced on AM-aluminum alloys, Key Eng. Mater. 813 (2019) 298–303.
[27] J.F. Moulder, W.F. Stickle, P.E. Sobol, K.D. Bomben, J. Chastain, Handbook of X-ray Photoelectron Spectroscop, Perkin Elemer Corp, Eden Prairie, MN, 1992.
[28] X-ray Photoelectron Spectroscopy Database 20, Version 4.1, National Institute of Standards and Technology, Gaithersburg.
[29] T.W. Clyne, S.C. Troughton, A review of recent work on discharge characteristics during plasma electrolytic oxidation of various metals, Int. Mater. Rev. 64 (2019) 127–162.
[30] L. Zhu, R.S. Petrova, J.P. Gashinski, Z. Yang, The effect of surface roughness on PEO-treated Ti-6Al-4V alloy and corrosion resistance, Surf. Coat. Technol. 325 (2017) 22–29.
[31] B. Yoo, K.R. Shin, D.Y. Hwang, D.H. Lee, D.H. Shin, Effect of surface roughness on leakage current and corrosion resistance of oxide layer on AZ91 Mg alloy prepared by plasma electrolytic oxidation, Appl. Surf. Sci. 256 (2010) 6667–6672.
[32] T. Wu, C. Blawert, M.L. Zheludkevich, Influence of secondary phases of AlSi9Cu3 alloy on the plasma electrolytic oxidation coating formation process, J. Mater. Sci. Technol. 50 (2020) 75–85.
[33] M.M. Krishtal, M.Y. Ryumkin, Inherited chemical inhomogeneity in oxide layers deposited by the method of microarc oxidizing on hypereutectic silumins, Met. Sci. Heat Treat. 49 (2007) 111–117.
[34] V. Dehnavi, B.L. Luan, D.W. Shoesmith, X.Y. Liu, S. Rohani, Effect of duty cycle and applied current frequency on plasma electrolytic oxidation (PEO) coating growth behavior, Surf. Coat. Technol. 226 (2013) 100–107.
[35] V. Dehnavi, X. Yang Liu, B. Li Luan, D.W. Shoesmith, S. Rohani, Phase transformation in plasma electrolytic oxidation coatings on 6061 aluminum alloy, Surf. Coat. Technol. 251 (2014) 106–114.
[36] P. Cerchier, L. Pezzato, K. Brunelli, P. Dolcet, A. Bartolozzi, R. Bertani, M. Dabalà, Antibacterial effect of PEO coating with silver on AA7075, Mater. Sci. Eng. C 75 (2017) 554–564.
[37] L. Pezzato, M. Rigon, A. Martucci, K. Brunelli, M. Dabalà, Plasma Electrolytic Oxidation (PEO) as pre-treatment for sol-gel coating on aluminum and magnesium alloys, Surf. Coat. Technol. 366 (2019) 114–123.
[38] R. Arrabal, B. Mingo, A. Pardo, M. Mohedano, E. Matykina, M.C. Merino, A. Rivas, Microstructure and corrosion behaviour of A356 aluminium alloy modified with Nd, Mater. Corros. 66 (2015) 535–541.
[39] D. Kong, C. Dong, X. Ni, X. Li, Corrosion of metallic materials fabricated by selective laser melting, Mater. Degrad. 3 (2019) 24.
[40] L. Pezzato, R. Babbolin, P. Cerchier, M. Marigo, P. Dolcet, M. Dabalà, K. Brunelli, Sealing of PEO coated AZ91magnesium alloy using solutions containing neodymium, Corros. Sci. 173 (2020) 108741.
[41] S. Menargues, J.A. Picas, E. Martin, M.T. Baile, M. Campillo, A. Forn, Surface finish effect on the anodizing behaviour of Al-Si components obtained by sub-liquidus casting process, Int. J. Mater. Form. 3 (2010) 767–770.
[42] D. Caliari, G. Timelli, T. Salata, G. Cavagnini, S. Maestri, A. Manfredini, Influence of microstructure and surface finishing on the hard anodizing of diecast Al-Si-Cu alloys, La Metal. Ital. 4 (2019) 23–31.
[43] M. Mohedano, E. Matykina, R. Arrabal, B. Mingo, M.L. Zheludkevich, PEO of rheocast A356 Al alloy: energy efficiency and corrosion properties, Surf. Interface Anal. 48 (2015) 953–959.
[44] M. Mohedano, E. Matykina, R. Arrabal, B. Mingo, A. Pardo, PEO of pre-anodized Al - Si alloys: corrosion properties and influence of sealings, Appl. Surf. Sci. 346 (2015) 57–67.
[45] K. Li, W. Li, G. Zhang, W. Zhu, F. Zheng, D. Zhang, M. Wang, Effects of Si phase refinement on the plasma electrolytic oxidation of eutectic Al-Si alloy, J. Alloys Compd. 790 (2019) 650–656.